

# A MESHLESS FRONT TRACKING METHOD FOR THE EULER EQUATIONS OF FLUID DYNAMICS

**Jeroen A.S. Witteveen**

Department of Aerodynamics,  
Faculty of Aerospace Engineering,  
Delft University of Technology, The Netherlands  
j.a.s.witteveen@tudelft.nl

## Abstract

*A second order front tracking method is developed for solving the Euler equations of inviscid fluid dynamics numerically. Front tracking methods are usually limited to first order accuracy, since they are based on a piecewise constant approximation of the solution. Here the second order convergence is achieved by building a piecewise linear reconstruction of the piecewise constant front tracking solution in a post-processing step. The linearization is performed by decomposing the piecewise constant solution of the hyperbolic system into its wave components and by linearizing the wave solutions separately. In order to achieve a physically correct linearization, the front types of the previously developed improved front tracking method are employed. It is illustrated numerically for the one-dimensional unsteady interacting blast waves problem and a two-dimensional supersonic airfoil flow validation study that the proposed front tracking method can achieve second order convergence also in the presents of strong discontinuities.*

*Key words: Front tracking, Second order, Meshless methods, Euler equations*

## 1 Introduction

Front tracking is an effective tool for solving hyperbolic conservation laws in the presence of strong discontinuities. Often a type of front tracking method is used that models the discontinuities by separate degrees of freedom in addition to a fixed background mesh for capturing the continuous phenomena as introduced by Richtmyer and Morton [10].

Also meshless front tracking methods have been developed which resolve both the discontinuities and the continuous regions of the solution domain [6]. This type of methods initiated by Risebro and Tveito [12] do not require a background mesh by approximating continuous phenomena using a series of small discontinuities. The latter type of front tracking methods has been used as an analytical tool for studying scalar equations and systems of hyperbolic conservation laws in for example [1,2,4]. In this paper the class of meshless front tracking methods is considered as a numerical approach for solving the hyperbolic Euler equations of inviscid fluid mechanics.

Meshless front tracking methods are based on the piecewise constant approximation of the solution of local Riemann problems. The Riemann problems originate from discontinuities in a piecewise constant approximation of the initial conditions of an initial-boundary value problem. The piecewise constant solution of these local Riemann problems results in the introduction of new discontinuities. The location of these moving discontinuities in the space-time domain is tracked by fronts. At an intersection of two fronts, the front interaction is governed by the new local Riemann problem, and so on.

This front tracking method has been applied to one-dimensional problems in shallow water flows, gas dynamics, and polymer flooding in [3,7,11]. One-dimensional front tracking is of interest for, for example, pipe flows and shock tube problems. An equivalent algorithm can also be used to simulate two-dimensional supersonic flows [15]. The dimensional splitting techniques has been used to extend front tracking to higher dimensions by Holden, Lie, et al. [5,8].

Recently an improved front interaction model was proposed for a physically more accurate simulation of the Euler equations [15]. The model employs the wave phenomena of the intersecting fronts to better predict the wave pattern created at the front interaction based on gas dynamics theory. To that end, wave front types are used to track the physical phenomena that the fronts represent.

Due to the piecewise constant approximation of the solution, front tracking methods usually result in first order error convergence [12]. It is known that, although a piecewise constant approximation results locally in a first order error, integral quantities can be approximated with second order accuracy. This was numerically illustrated for the conservation of mass, momentum, and energy [15], and the location of the fronts [14]. A fully second order front tracking method for scalar conservation laws in one dimension has been developed by Lucier [9] based on a piecewise linear approximation.

In this paper, a second order front tracking method for the system of Euler equations is proposed based on the front types of the improved front tracking method [15]. The second order accurate solution is obtained by a *a posteriori* piecewise linear reconstruction of the piecewise constant front tracking solution. In contrast to scalar equations, systems of conservation laws allow for multiple wave families which can coexist in any location in space-time. The piecewise linear approximation is, therefore, constructed by decomposing the front tracking solution into a series of wave solutions and by linearizing these wave solutions separately. This approach is based on the observation that, although the nonlinear problem itself cannot be *solved* by summing wave solutions, the front tracking solution can nonetheless be *decomposed* into a summation of wave solutions. The front types of the improved front tracking method are employed in this linearization to obtain a physically accurate reconstruction.

The formulation of the developed piecewise linear front tracking method is presented in section 2. The two intersecting blast waves benchmark problem is considered in section 3 to illustrate the properties of the method in case of strong discontinuities. In section 4 results for a two-dimensional supersonic airfoil flow application are validated in comparison to experimental data. The main conclusions are summarized in section 5.

## 2 Second order front tracking for the Euler equations

Standard front tracking for the Euler equations is briefly reviewed in section 2.1. In section 2.2 the formulation of the improved front tracking method is revisited. The second order extension based on piecewise linear reconstruction is introduced in section 2.3.

### 2.1 Meshless front tracking

The Euler equations for one-dimensional unsteady inviscid flow without heat conduction are given in the conservation formulation by

$$\frac{\partial U}{\partial t} + \frac{\partial F(U)}{\partial x} = 0, \quad (1)$$

where

$$U = \begin{pmatrix} \rho \\ \rho u \\ \rho E \end{pmatrix}, \quad F = \begin{pmatrix} \rho u \\ \rho u^2 + p \\ \rho u H \end{pmatrix}, \quad U(x,0) = U_0(x), \quad (2)$$

with state vector  $U(x,t)$ , flux vector  $F(x,t)$ , and initial condition  $U_0(x)$  in terms of density  $\rho(x,t)$ , velocity  $u(x,t)$ , static pressure  $p(x,t)$ , total energy  $E(x,t)$ , and enthalpy  $H(x,t)$  as function of spatial coordinate  $x \in \mathcal{R}$  and time  $t \in \mathcal{R}^+$ . A perfect gas is considered for which holds  $E = (1/(\gamma-1))p/\rho + u^2/2$  and  $H = E + p/\rho$ , with ratio of specific heats  $\gamma = c_p/c_v$ .

A front tracking method approximates the solution of (1) in the space-time plane by a piecewise constant function based on uniform flow conditions  $U_i$  in  $n_{\text{cells}}$  cells  $A_i$  with  $i=1, \dots, n_{\text{cells}}$ . The cell boundaries are composed of  $n_{\text{fronts}}$  linear front paths  $f_i$  with  $i=1, \dots, n_{\text{fronts}}$ , where the fronts constitute

physical wave phenomena, such as shock waves, contact waves, and characteristics. The starting and end points of the front paths  $f_i$  form a set of  $n_{\text{nodes}}$  nodes  $p_i=(x_{p,i}, t_{p,i})$  in space-time with  $i=1, \dots, n_{\text{nodes}}$ . Pointers are used to establish the relation between cells  $A_i$  and fronts  $f_i$ , and fronts  $f_i$  and nodes  $p_i$ .

The first step in a meshless front tracking algorithm is the piecewise constant discretization of the initial conditions  $U_0(x)$ . The discontinuities at the nodes  $p_i$  in these discretized flow conditions resemble locally the initial conditions of a Riemann problem given by

$$U_0 = \begin{cases} U^-, & x < 0, \\ U^+, & x \geq 0, \end{cases} \quad (3)$$

with  $U^-$  and  $U^+$  the constant left and right states, respectively. The simulation is then initiated by solving the local Riemann problems at the nodes  $p_i$  in the discretized initial conditions. The piecewise constant approximation of the solutions of the Riemann problems leads to the creation of cells  $A_i$  and fronts  $f_i$  with front velocities  $u_{f,i}$ , which are constant in time. In nonlinear problems the front velocities  $u_{f,i}$  are in general different for different fronts. At the location of the intersection of fronts in space-time, a new node  $p_i$  is created and a local Riemann problem is again solved, and so on until a certain time  $t=t_{\text{stop}}$  is reached. The accuracy of the simulation is mainly governed by the number of fronts  $n_f$  that is used to discretize the rarefaction fans. The number of fronts can also be chosen adaptively based on the strength of the rarefaction fan using a discretization parameter  $\delta$ . The resulting piecewise constant approximation converges with first order accuracy [6]. Usually only interactions of two fronts are considered without loss of generality.

## 2.2 Formulation of the improved front tracking algorithm

In the improved front tracking method for the Euler equations [15] a better physical modeling of the front interactions is obtained by explicitly taking into account the wave phenomena that the fronts represent. The following front types  $f_{\text{type},i}$  are used to track the wave phenomena of the fronts

$$f_{\text{type},i} \in \{sw, lch, ich, rch, cd, lcw, icw, rcw\}, \quad (4)$$

for  $i=1, \dots, n_{\text{fronts}}$ . The front types distinguish between shock waves (sw), left/internal/right characteristics of a fan of characteristics (lch/ich/rch), contact discontinuities (cd), and left/internal/right contact waves of a region of continuous change of entropy (lcw/icw/rcw). Also front families

$$f_{\text{family},i} \in \{-1, 0, 1\}, \quad (5)$$

for  $i=1, \dots, n_{\text{fronts}}$ , are assigned to the fronts to denote left running  $-1$ , right running  $1$ , and convective  $0$  fronts. The front type  $f_{\text{type},i}$  and front family  $f_{\text{family},i}$  govern both the relation for the front velocity  $u_{f,i}$  and the interaction with other fronts in the improved front interaction model. The front interaction model prescribes the wave types

$$w_{\text{type},k} \in \{sw, lch, ich, rch, cd, lcw, icw, rcw, crw\}, \quad (6)$$

with  $k \in \{\text{left}, \text{middle}, \text{right}\}$ , of the created left, middle, and right waves at a front interaction as function of the front types  $f_{\text{type},i}$  and wave families  $f_{\text{family},i}$  of the two intersecting fronts,  $i_{\text{left}}$  and  $i_{\text{right}}$ . Wave types  $w_{\text{type},k}$  differ from front types  $f_{\text{type},i}$  in the sense that the former include centered rarefaction waves (crw). A centered rarefaction wave (crw) is discretized by a series of fronts representing characteristics (lch/ich/rch). The model consists of three tabulated functions  $g_k$ , for which holds

$$w_{\text{type},k} = g_k \left( f_{\text{type},i_{\text{left}}}, f_{\text{type},i_{\text{right}}}, f_{\text{family},i_{\text{left}}}, f_{\text{family},i_{\text{right}}} \right) \quad (7)$$

with  $k \in \{\text{left, middle, right}\}$ . The functions  $g_k$  are derived from theoretical gas dynamics and are given in tabulated form in [15]. The front types  $f_{\text{type},i}$  of the fronts created at the intersection point are then derived from the created wave types  $w_{\text{type},k}$  as follows

$$f_{\text{type},i} \begin{cases} = w_{\text{type},k}, & w_{\text{type},k} \neq \text{crw}, \\ \in \{\text{lch, ich, rch}\}, & w_{\text{type},k} = \text{crw}. \end{cases} \quad (8)$$

The front families  $f_{\text{family},i}$  are determined by whether a front is created as part of a left, middle, or right wave at a front interaction

$$f_{\text{family},i} = \begin{cases} -1, & k = \text{left}, \\ 0, & k = \text{middle}, \\ 1, & k = \text{right}. \end{cases} \quad (9)$$

A non-standard Riemann solver, which takes into account whether the created wave types  $w_{\text{type},k}$  are isentropic or possibly non-isentropic, is used to determine the velocity of the created fronts  $u_{\text{front},i}$  and the flow conditions in the created cells  $U_i$ . If the created wave type is a shock wave  $w_{\text{type},k} = \text{sw}$  but the Riemann solver predicts an expansion, then the created wave is represented by a centered rarefaction wave,  $w_{\text{type},k} = \text{crw}$ .

### 2.3 Second order piecewise linear reconstruction

A second order accurate front tracking solution is obtained by using a piecewise linear reconstruction of the original piecewise constant front tracking approximation in a post-processing step. The piecewise linear solution is constructed by decomposing the front tracking approximation into a summation of wave components and by linearizing each wave solution separately. In order to decompose the piecewise constant approximation into its  $n_{\text{wave}}$  wave solutions, the waves present in the flow are numbered by wave numbers  $\text{wave}_{\text{number},m}$ , with  $m=1, \dots, n_{\text{waves}}$ . A wave can in this context be a shock wave, a fan of characteristics, a contact discontinuity, or a region of continuous change of entropy. In order to track which fronts belong to which wave, the wave numbers  $\text{wave}_{\text{number},m}$  are assigned to the fronts in the form of front numbers  $f_{\text{number},i}$ , with  $i=1, \dots, n_{\text{fronts}}$ , for which holds

$$f_{\text{number},i} = \text{wave}_{\text{number},m}, \quad (10)$$

if front  $i$  is part of wave  $m$ . Based on the numbering of the fronts by the wave numbers, the solution  $U(x)$  at  $t=t_{\text{stop}}$  is decomposed into a series of wave solutions  $V_m(x)$ , for  $m=1, \dots, n_{\text{waves}}$ ,

$$U(x) = U_{\text{ref}} + \sum_{m=1}^{n_{\text{waves}}} V_m(x), \quad (11)$$

where for the reference value holds  $U_{\text{ref}} = U(x_{\text{ref}})$  with  $x_{\text{ref}}$  the left most point of the spatial domain. The individual wave solutions  $V_m(x)$  are then linearized to obtain the linear wave solutions  $W_m(x)$  while taking into account the front types  $f_{\text{type},i}$  for  $f_{\text{number},i} = \text{wave}_{\text{number},m}$  and  $m=1, \dots, n_{\text{waves}}$  to obtain a physically correct linearization. The piecewise linear solution  $U_{\text{lin}}(x)$  at  $t=t_{\text{stop}}$  is finally obtained by summing the linearized wave solutions  $W_m(x)$

$$U_{\text{lin}}(x) = U_{\text{ref}} + \sum_{m=1}^{n_{\text{waves}}} W_m(x). \quad (12)$$

### 3 Two interacting blast waves problem

A classical test problem for assessing the performance of numerical methods in the presence of strong discontinuities is the two interacting blast waves problem introduced by Woodward [16]. The blast waves shock tube problem on the domain  $x=[0,1]$  is defined by the initial condition consisting of three uniform regions for the pressure

$$p = \begin{cases} 1000, & 0 < x < 0.1, \\ 0.01, & 0.1 < x < 0.9, \\ 100, & 0.9 < x < 1, \end{cases} \quad (13)$$

and constant velocity  $u=0$  and density  $\rho=1$  between reflecting walls at  $x=0$  and  $x=1$ . The solution until  $t=0.04$  involves the interaction of the strong shock waves and contact discontinuities with the reflections of the rarefaction waves created at the jumps in the initial condition. This results in a highly complex interaction in the collision region as illustrated by the space-time front tracking solution for a discretization of the rarefaction waves with  $\delta=0.1$  in Figure 1a. The piecewise linear front tracking solution of the density  $\rho$ , velocity  $u$ , and pressure  $p$  at  $t=0.038$  for  $\delta=0.05$  of Figures 1b to 1d gives a smooth approximation of the continuous regions and a sharp resolution of the discontinuities. The predicted flow field shows excellent agreement to the benchmark results presented in [17].

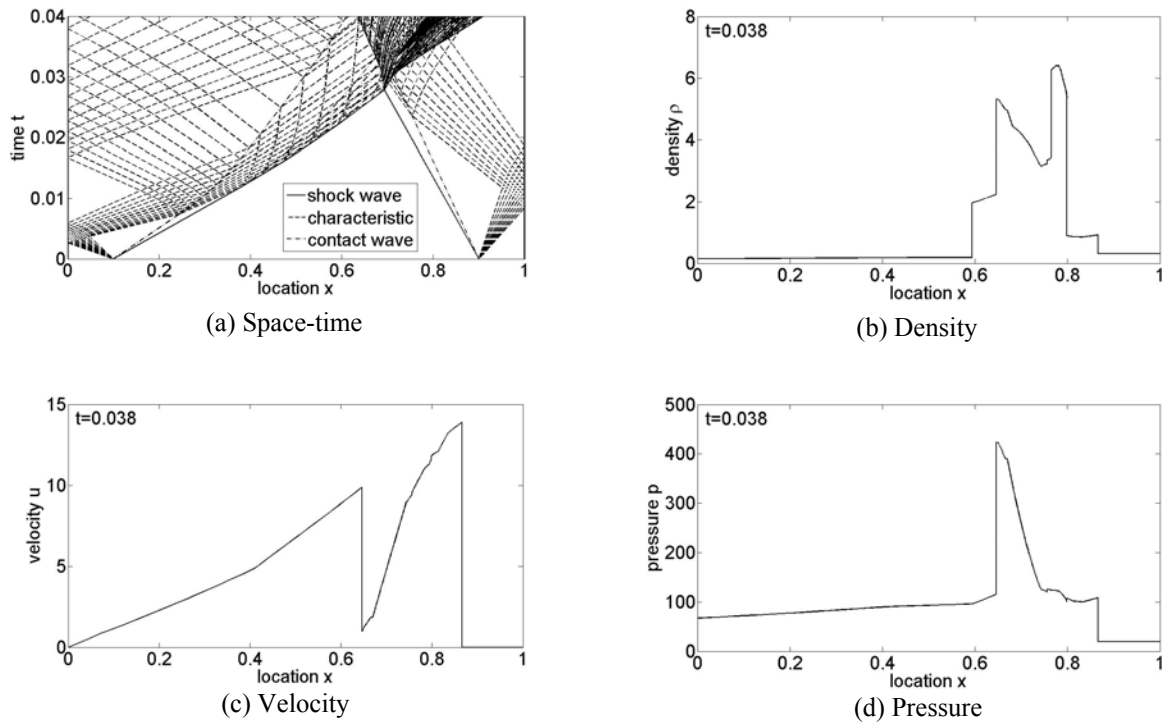


Figure 1 Solution of the two interacting blast waves problem up to  $t=0.04$  for  $\delta=0.1$  and at  $t=0.038$  for  $\delta=0.05$ .

The time evolution of the density  $\rho$  between  $t=0$  and  $t=0.038$  at times also considered in [17] is given in Figure 2. Initially for  $t \leq 0.026$  the density shows two separated left and right wave patterns with strong discontinuities emanating from the left and right discontinuity in the initial conditions resulting in a maximum density of  $\rho=6.0$ . After the intersection of the two shock waves the density peaks at  $\rho=28.52$  for  $t=0.028$  and decreases with increasing time. The error convergence for  $u$ ,  $p$ , and  $\rho$  of piecewise linear front tracking is compared in Figure 3 to that of piecewise constant front tracking as function of  $\delta$ . The results for  $t \leq 0.026$  before the collision of the shock waves clearly illustrate that the piecewise linear approximation can achieve second order convergence also in this problem with strong discontinuities. After the shock wave collision for  $t \geq 0.028$  lower values of discretization parameter  $\delta$  are required to start to reach second order convergence due to the higher detail in the

complex solution at these times. The piecewise linear front tracking method consistently achieves higher convergence rates and lower errors than the first order piecewise constant front tracking method.

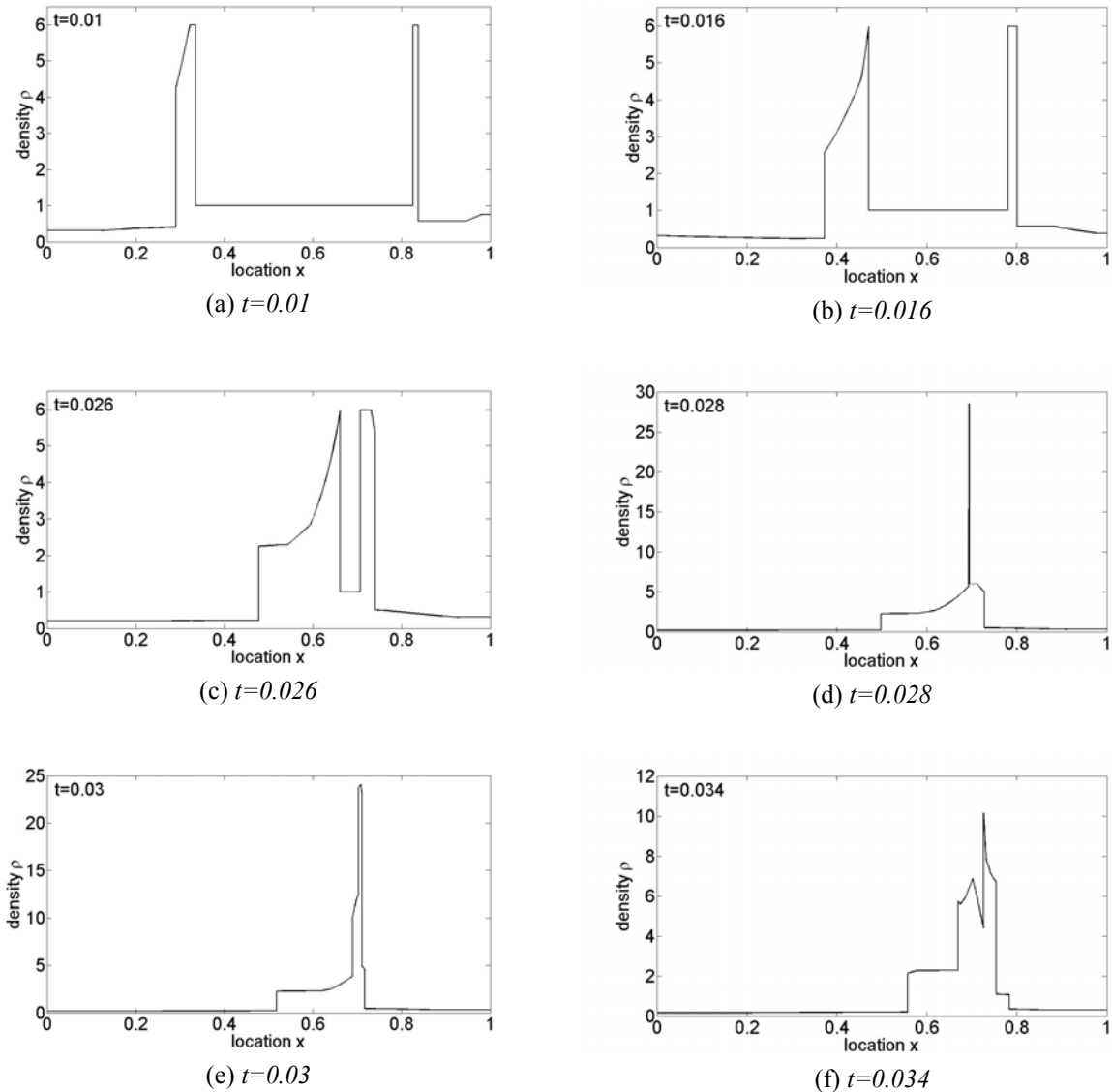


Figure 2 Density of the two interaction blast waves problem at  $t=0.038$  for  $\delta=0.05$ .

#### 4 Two-dimensional supersonic airfoil flow

The meshless front tracking method is also an effective approach for simulating two-dimensional supersonic steady Euler flows. In that case the free stream flow direction instead of the time axis is treated as the hyperbolic coordinate. This approach is applicable if the velocity component in the direction of the undisturbed flow streamlines is supersonic throughout the whole flow field. This implies, for example, an airfoil flow with attached shock waves at the sharp leading and trailing edges of the airfoil with sufficiently small thickness and angle of attack. In [15] a two-dimensional front tracking algorithm was considered previously in a piecewise constant formulation and only for zero angle of attack. Here the piecewise linear front tracking method is applied to predict the lift-drag curve of a supersonic airfoil over a range of angles of attack.

In the Euler equations for two-dimensional supersonic flow an additional variable for the velocity component  $v$  in the  $y$ -direction perpendicular to the free stream flow direction coordinate  $x$  is introduced. The resulting equations are in a similar notation as the one-dimensional Euler equations (1) given by

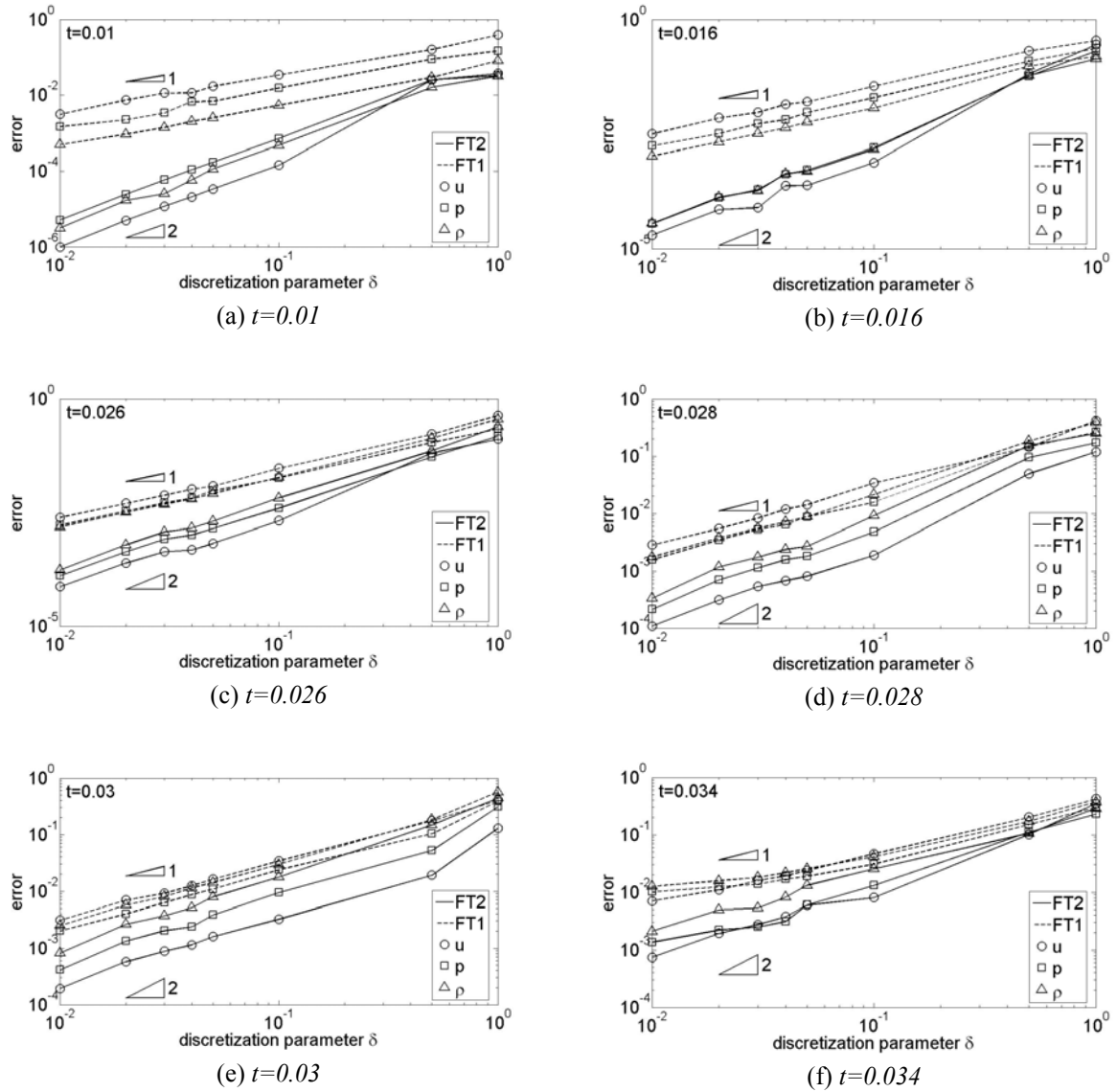


Figure 3 Error convergence of the piecewise linear (FT2) and piecewise constant (FT1) front tracking method for the two interacting blast waves problem.

$$\frac{\partial F}{\partial x} + \frac{\partial G}{\partial y} = 0, \quad (14)$$

with

$$F = \begin{pmatrix} \rho u \\ \rho u^2 + p \\ \rho uv \\ \rho uH \end{pmatrix}, \quad G = \begin{pmatrix} \rho v \\ \rho uv \\ \rho v^2 + p \\ \rho vH \end{pmatrix}. \quad (15)$$

The front tracking algorithm requires only minor modifications to be able to solve these two-dimensional Euler equations. The value of the additional unknown  $v$  has to be stored for every cell and the one-dimensional Riemann solvers have to be replaced by their two-dimensional supersonic counterparts. The wave types and the front interaction tables remain unchanged.

The considered geometry is a symmetrical circular-arc airfoil with chord length  $c=0.1\text{m}$  and 12% thickness. The constant curvature of the airfoil defined by a radius of curvature of  $R=0.21133\text{m}$  results

in a leading and trailing edge semi-opening angle of  $\theta_0=13.69\text{deg}$ . In order to solve the airfoil flow problem for non-zero angle of attack the flow domain is divided into the three subdomains shown in Figure 4. The three domains are separated by a horizontal line from the leading edge pointing in the upstream direction and a vertical line through the trailing edge. The flow in the resulting domains *I* and *II* can be resolved independently from each other and potentially in parallel due to the hyperbolicity of the problem. The solutions of *I* and *II* at the  $x$ -coordinate of the trailing edge are used as boundary condition for domain *III*, which contains the trailing edge shocks and the inviscid entropy wake behind the airfoil. For computing the aerodynamic forces on the airfoil using surface pressure integration it is sufficient to consider domains *I* and *II* only.

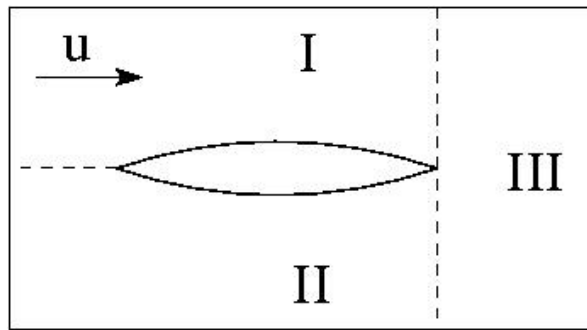


Figure 4 Spatial domain decomposition for the two-dimensional supersonic airfoil flow.

The flow solutions for two cases with different free stream Mach numbers  $M_\infty=2$  and  $M_\infty=2.5$  and angle of attack  $\alpha=5\text{deg}$  are given in Figure 5 in terms of the Mach number field and the computational grid for a discretization of the airfoil with 40 points at each side. The piecewise linear front tracking results show a sharp resolution of the curved leading and trailing edge shock waves. The case for  $M_\infty=2.5$  results in sharper shock wave angles with respect to the free stream flow direction and a larger range of Mach numbers in the flow field. Figures 5c and 5d illustrate the highly efficient discretization of the spatial flow domain with only two cells for representing the undisturbed flow upstream of the leading edge shock waves. The curvature of the shock waves is resolved by the interaction of the shock waves with the rarefaction characteristics emanating from the airfoil surface. This results in the creation of reflected characteristics and contact waves. These secondary phenomena also result in the prediction of the non-uniform flow conditions downstream of the trailing edge shock waves.

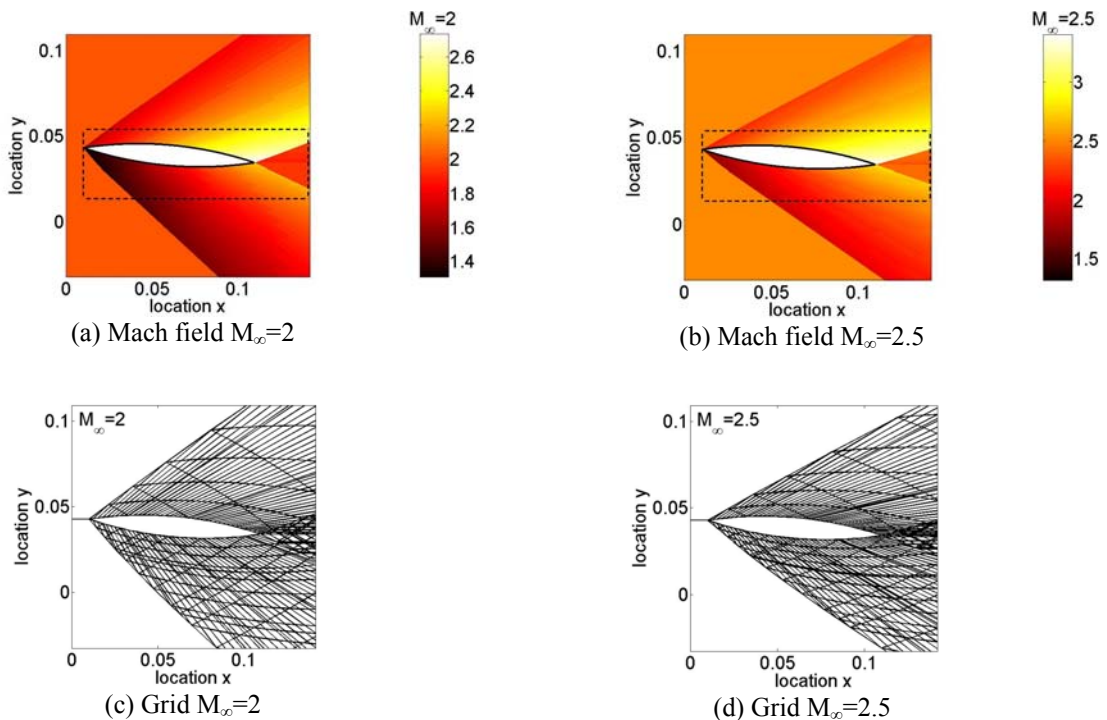


Figure 5 Mach field and grid for the two-dimensional supersonic airfoil flow.

The rectangular contour in Figures 5a and 5b denotes the integration contour used in an experimental campaign for PIV based load determination of the same configuration by Souverein et al. [13]. The PIV velocity measurements are based on illumination of 50nm TiO<sub>2</sub> seeding particles in a 1.5mm thick light sheet produced by a Big Sky Laser CFR PIV-200 Nd:YAG with a 532nm wavelength, 200mJ/pulse energy, and 6ns pulse duration. The 146.5mm×80.1mm field of view is imaged with a 1280×1024 pixel CCD camera where the vertical size is cropped to 800 pixels.

The validation comparison of the computed flow conditions and the measured velocities along the contour is given in Figure 6. The flow conditions along the contour are displayed in clockwise direction starting at the top left corner as function of the curvilinear abscissa normalized by the airfoil chord  $s/c$ . The dotted vertical lines indicate the location of the corners of the integration contour. The velocity components predicted by the front tracking solution of the Euler equations closely agree with the experimental data which indicates that viscous effects are generally small in this flow problem. The numerical and experimental results also show the same trends for the velocity components as function of the Mach number. The numerical solution shows clearly the inviscid entropy wake behind the airfoil for the streamwise velocity component  $u$ . The entropy wake is largest behind the upper surface due to the high pre-shock Mach number in combination with the relatively high curvature of this trailing edge shock wave. The slip line emanating from the trailing edge of the airfoil is also resolved as a true discontinuity. In the experimental results the local effect of the viscous wake can be recognized.

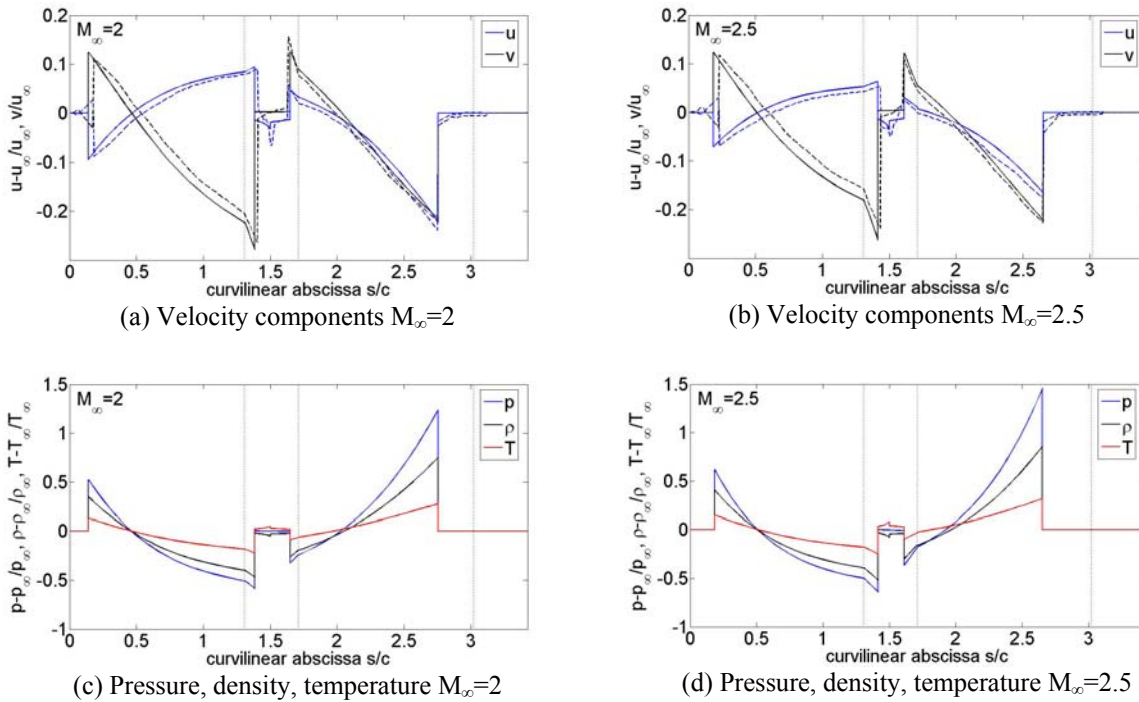


Figure 6 Computed flow conditions and measured velocity components (dashed lines) on the integration contour for the two-dimensional supersonic airfoil flow.

Finally the lift-drag curve of the airfoil for angles of attack between  $\alpha=0\text{deg}$  and  $\alpha=6\text{deg}$  is considered in Figure 7 based on pressure integration over the airfoil surface in terms of the lift and drag coefficients

$$C_l = \frac{L}{\frac{1}{2} \rho_\infty u_\infty^2 c}, \quad C_d = \frac{D}{\frac{1}{2} \rho_\infty u_\infty^2 c}, \quad (16)$$

with lift and drag forces  $L$  and  $D$ . As an illustration the second order convergence of  $C_l$  and  $C_d$  for  $M_\infty=2$  and  $\alpha=5\text{deg}$  is given in Figure 7a for an increasing number of airfoil surface discretization points with respect to a finer reference solution. The lift-drag curve of Figure 7b shows the typical

parabolic trend with lower lift and drag coefficients for the higher Mach number of  $M_\infty=2.5$  in the considered range of angles of attack.

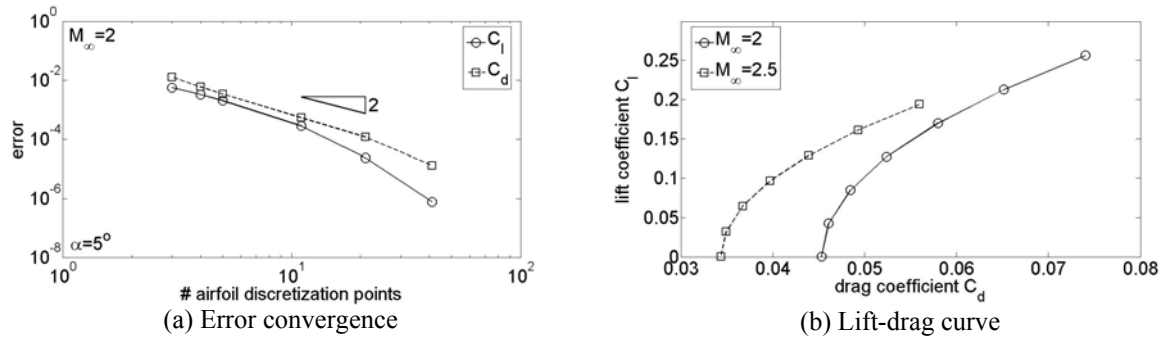


Figure 7 Lift and drag coefficients for the two-dimensional supersonic airfoil flow.

## 5 Conclusions

A second order front tracking method is presented for the numerical treatment of the Euler equations. The second order convergence is obtained by linearizing the piecewise constant front tracking solution in a post-processing step. The piecewise linear solution is obtained by first decomposing the front tracking approximation in wave solutions. The wave solutions are then linearized separately based on the physical phenomena that the fronts represent as tracked by the front types of the improved front tracking method.

The piecewise linear front tracking method is applied to two-dimensional hyperbolic Euler flow problems. The error convergence study for the two interacting blast waves problem shows a second order accuracy also for the interaction of strong discontinuities. The flow solutions illustrate the sharp resolution of discontinuities and the smooth approximation of continuous flow phenomena.

The validation study for a two-dimensional supersonic airfoil flow over the range of angles of attack up to  $\alpha=6\text{deg}$  and for Mach numbers  $M_\infty=2$  and  $M_\infty=2.5$  shows a good agreement with the experimental data. The resulting computational grids illustrate the highly efficient discretization of the spatial flow domain by the front tracking method. The predicted lift and drag coefficients in the lift-drag diagram also show a second order convergence rate.

## Acknowledgement

The author would like to acknowledge L.J. Souverein, B.W. van Oudheusden, and F. Scarano for providing the experimental PIV velocity measurements in the collaborative validation study for the two-dimensional supersonic airfoil flow problem.

## References

- [1] P. Baiti, H.K. Jenssen, On the front tracking algorithm, *Journal of Mathematical Analysis and Applications*, 217, 395-404, 1998.
- [2] A. Bressan, P. LeFloch, Uniqueness of weak solution to systems of conservation laws. *Archive for Rational Mechanics and Analysis*, 140, 301-317, 1997.
- [3] R. Holdahl, H. Holden, K.-A. Lie, Unconditionally stable splitting methods for the shallow water equations. *BIT Numerical Mathematics*, 39, 451-472, 1999.
- [4] H. Holden, N.H. Risebro, A method of fractional steps for scalar conservation laws without the CFL condition. *Mathematics of Computation*, 60, 221-232, 1993.
- [5] H. Holden, K.-A. Lie, N.H. Risebro, An unconditionally stable method for the Euler equations. *Journal of Computational Physics*, 150, 76-96, 1999.
- [6] H. Holden, N.H. Risebro, *Front tracking for hyperbolic conservation laws*, Springer-Verlag, New York, 2002.
- [7] J.O. Langseth, N.H. Risebro, A. Tveito, A conservative front tracking scheme for 1D hyperbolic conservation laws. In: *Nonlinear Hyperbolic Problems: Theoretical, Applied, and Computational*

- Aspects, A. Donato et al., Eds., Notes on Numerical Fluid Mechanics, 43, Vieweg, Braunschweig, 385, 1993.
- [8] K.-A. Lie, V. Hauge, K. Hvistendahl Karlsen, Dimensional splitting with front tracking and adaptive grid refinement. *Numerical Methods for Partial Differential Equations*, 14, 627-648, 1998.
- [9] Lucier, A moving mesh numerical method for hyperbolic conservation laws. *Mathematics of Computation*, 173, 59-69, 1986.
- [10] R. Richtmyer, K. Morton, *Difference methods for initial value problems*, Interscience, New York, 1967.
- [11] N.H. Risebro, A. Tveito, Front tracking applied to a nonstrictly hyperbolic system of conservation laws. *SIAM Journal on Scientific and Statistical Computing*, 12, 1401-1419, 1991.
- [12] N.H. Risebro, A. Tveito, A front tracking method for conservation laws in one dimension. *Journal of Computational Physics*, 101, 130-139, 1992.
- [13] L.J. Souverein, B.W. van Oudheusden, F. Scarano, Particle image velocimetry based loads determination in supersonic flows. *AIAA-2007-50*, 45th AIAA Aerospace Sciences Meeting and Exhibit, Reno, Nevada, 2007.
- [14] J.A.S. Witteveen, A second-order front tracking method applied to the Euler equations. *AIAA-2006-1277*, 44th AIAA Aerospace Sciences Meeting and Exhibit, Reno, Nevada, 2006.
- [15] J.A.S. Witteveen, B. Koren, P.G. Bakker, An improved front tracking method for the Euler equations. *Journal of Computational Physics*, 224, 712-728, 2007.
- [16] P.R. Woodward, Trade-offs in designing explicit hydrodynamics schemes for vector computers. In: *Parallel Computation*, G. Rodrigue, Ed., Academic Press, New York, 1982.
- [17] P.R. Woodward, P. Colella, The numerical simulation of two-dimensional flow with strong shocks. *Journal of Computational Physics*, 54, 115-173, 1984.